Journal of Medicinal Chemistry

Article

Fragment-based discovery of a qualified hit targeting the Latency-associated Nuclear Antigen of the oncogenic Kaposi's Sarcoma-associated Herpesvirus/Human Herpesvirus 8

Philine Elea Kirsch, Valentin Jakob, Kevin Oberhausen, Saskia Stein, Ivano Salvatore Cucarro, Thomas F. Schulz, and Martin Empting

J. Med. Chem., **Just Accepted Manuscript** • DOI: 10.1021/acs.jmedchem.8b01827 • Publication Date (Web): 19 Mar 2019

ACS Publications

is published by the American Chemical Society. 1155 Sixteenth Street N.W., Washington, DC 20036

Fragment-based discovery of a qualified hit targeting the Latency-associated Nuclear Antigen of the oncogenic Kaposi's Sarcoma-associated Herpesvirus/Human Herpesvirus 8

*Philine Kirsch†[1,2,3], Valentin Jakob[1,2], Kevin Oberhausen[1,2], Saskia C. Stein[3,4], Ivano Cucarro[1,2], Thomas F. Schulz[3,4], Martin Empting[1,2,3]**

[1]Helmholtz-Institute for Pharmaceutical Research Saarland (HIPS)-Helmholtz Centre for Infection Research (HZI), Department of Drug Design and Optimization (DDOP), Campus E8.1, 66123 Saarbrücken, Germany

[2]Department of Pharmacy, Saarland University, Campus E8.1, 66123 Saarbrücken, Germany

[3]German Centre for Infection Research (DZIF), Partner Site Hannover-Braunschweig, Saarbrücken, Germany

[4]Institute of Virology, Hannover Medical School, Carl-Neuberg-Strasse 1, 30625 Hannover, Germany

ABSTRACT: The Latency-Associated Nuclear Antigen (LANA) is required for latent replication and persistence of Kaposi´s Sarcoma-associated Herpesvirus (KSHV)/human herpesvirus-8 (HHV-8). It acts via replicating and tethering the virus episome to the host chromatin and exert other functions. We conceived a new approach for the discovery of antiviral drugs to inhibit the interaction between LANA and the viral genome. We applied a biophysical screening cascade and identified the first LANA binders from small, structurally diverse compound libraries. Starting from a fragment-sized scaffold, we generated optimized hits via fragment growing using a dedicated fluorescence polarization-based assay as the structure-activity-relationship driver. We improved compound potency to the double-digit micromolar range. Importantly, we qualified the resulting hit through orthogonal methods employing EMSA, STD-NMR and MST methodologies. This optimized hit provides an ideal starting point for subsequent hit-to-lead campaigns providing evident target-binding, suitable ligand efficiencies and favorable physicochemical properties.

Introduction

Kaposi's sarcoma-associated herpesvirus (KSHV; taxonomic name human herpesvirus 8) is a human gamma herpes virus and is classified as a carcinogenic agent Group I by the World Health Organisation.[1; 2] It was identified as the etiological agent of Kaposi Sarcoma (KS) and lymphoproliferative disorders. After a first infection, it establishes a lifelong latent infection in the host organism. KSHV is usually not pathogenic in healthy individuals, but AIDS-related Kaposi's sarcoma (AIDS-KS), KS in transplant recipients and endemic KS in East/Central Africa cause significant morbidity and mortality in affected patients.[3] In latently infected cells, KSHV expresses only a limited set of proteins, which are important for the persistence. One of these is the Latency-Associated Nuclear Antigen (ORF73/LANA).[4,5] LANA plays an important role for the latency and regulation of the viral genome in the host organism. Previous studies have shown that LANA exerts several functions in the host cell like cell survival, transcriptional control, latent viral DNA replication and stable episome segregation during mitosis.[6] The *C*-terminal domain of LANA binds to the terminal repeat (TR) region of the viral genome in a sequence-specific manner. [7; 2] The TR consists of three adjacent LANA binding sites (LBS), which are referred to as LBS1, LBS2 and LBS3 (Figures 1 and 2).[7] The *N*-terminal domain of LANA is very poorly structured and is tethered to the host nucleosome.[8; 9] It is separated by a large internal repeat sequence from the *C*-terminal DNA-binding domain (Figure 1).[10; 11]

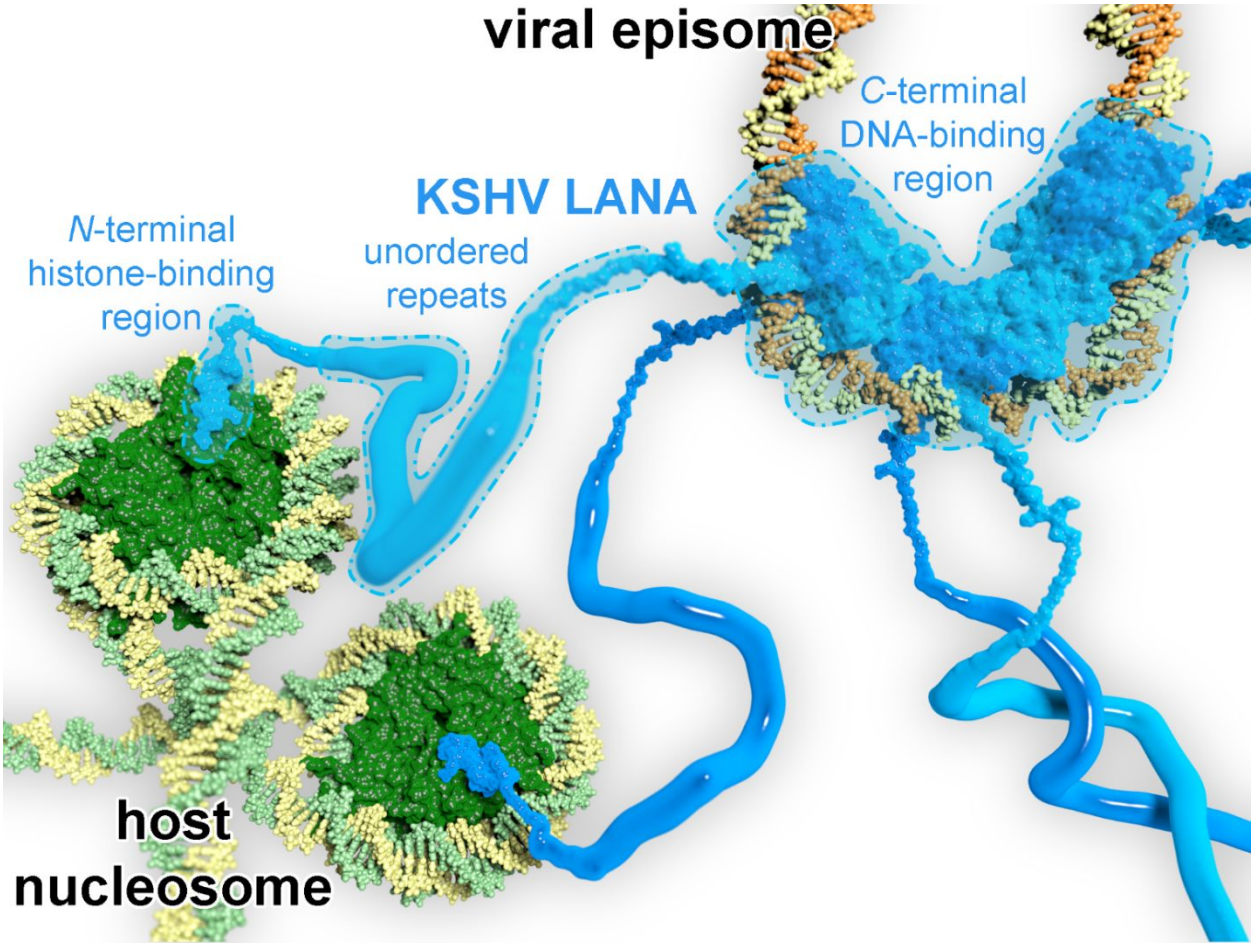

Figure 1. Illustration of molecular interactions between KSHV LANA, viral episome, and host nucleosome, rationalizing the *C*-terminal DNA binding domain of KSHV LANA as an antiviral drug target as it links viral DNA (yellow and orange) to host histones (dark green) and attached host DNA (yellow and green). Three KSHV LANA dimers (blue) are shown and unordered repeats are displayed as tubes. Illustration was modeled using coordinates of PDB entries 1zla, 4uzb and 4uzc.

To date, the options for treating KSHV-associated diseases are limited.[12] While several inhibitors of herpesviral DNA polymerases are active against KSHV productive replication, they are not effective against KS or other KSHV associated malignancies.[12] LANA represents a very promising target for the discovery and development of new anti-KSHV drugs that, in contrast to currently available compounds, would interfere with the latent phase of the viral life cycle. Based on the knowledge that LANA is involved in binding to viral latent episomal DNA and tethering it to host nucleosomes[7; 6] we conceived a new approach for the discovery of specific KSHV inhibitors. Our concept aims at the inhibition of the interaction between LANA and the viral genome. This should ultimately prevent latent persistence of KSHV, which could result in the gradual loss of infected cells and in a decrease in viral load in infected individuals. In the present work, we present our efforts to exploit this strategy through identification of the first functional LANA-DNA-interaction inhibitors by using fragment-based drug design. As a first step, we made use of different biological and biophysical methods to screen fragment libraries for identification of LANA binders. Subsequently, we established a fluorescence polarization-based assay to determine the inhibitory activity of our hits and we used it for further optimization steps. Furthermore, we confirmed target binding of our best compound via orthogonal assays using saturation-transfer difference (STD) NMR and microscale thermophoresis (MST) methodologies. Finally, we qualified the optimized hit scaffold for future lead-generation campaigns in an orthogonal interaction inhibition assay, namely electrophoretic mobility shift assay (EMSA). This provides an ideal starting point for subsequent medicinal-chemistry efforts toward specific anti-KSHV agents. To the best of our knowledge, this study is the first report of inhibitors targeting the DNA-binding domain of LANA. A similar approach, however, has been previously applied to the EBNA1 protein, the functional homologue of LANA in Epstein-Barr

virus (EBV).[13] However, these conceptually related studies as well as experiments with a DNA-binding site mutant of LANA provide a sufficient basis for the validity of this antiviral drug target.[14]

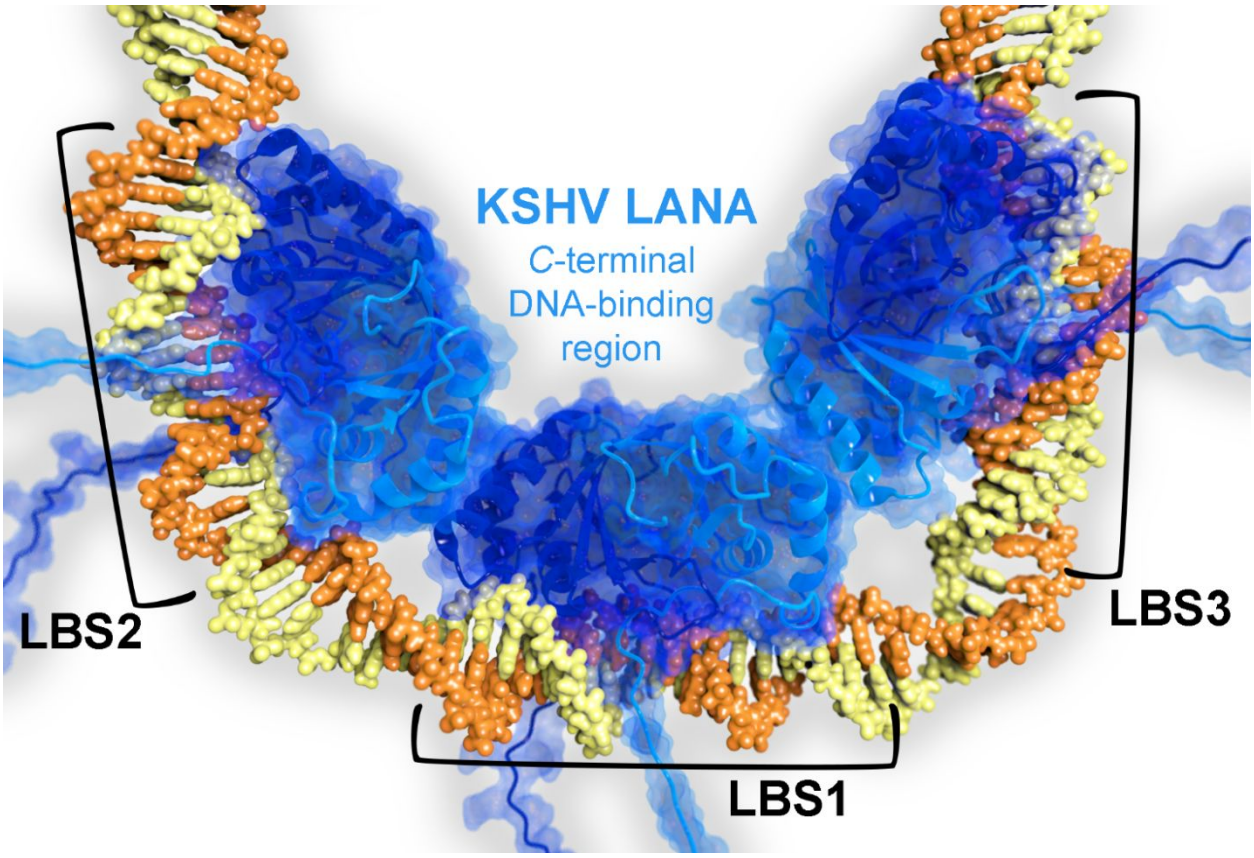

Figure 2. Model of the *C*-terminal DNA binding domain of three KSHV dimers bound to adjacent LANA-binding sites LBS1, 2, and 3. Protein chains are shown as ribbon representations (chain A: blue, chain B: light blue). Viral DNA (yellow orange) is shown in space-filling representation. The model was generated using pdb entries 4uzb and 4uzc.

Results and Discussion

Screening and Hit Identification. To discover the first small molecules, binding to LANA, we used orthogonal biophysical methods to screen two different small-molecule libraries from synthetic and natural sources.[15; 16] For the primary selection, we used two protein binding assays, surface plasmon resonance (SPR) and differential scanning fluorimetry (DSF) due to their high sensitivity and low protein consumption. First, we conducted SPR screening at a constant concentration to preselect putative LANA binders. Subsequently, we applied DSF ("Thermal Shift Assay" TSA) as a secondary filter.

This methodology enabled us to select 20 compounds for further testing. In order to test for functionality of our LANA binders in vitro, we established a fluorescence polarization-based assay, which allows for the quantitative evaluation of the LANA-DNA-interaction and its inhibition by small molecules. In this manner, we identified three promising small molecule hit scaffolds for further consideration. In this report, we will focus on our hit optimization efforts, starting from the fragment-sized Hit **1** (Figure 3).

SPR- and DSF-based Primary Screening. Two different libraries, containing a total of 720 highly structurally diverse set of hit-like small molecules with a molecular weight below 398 g/mol were screened.[15; 16] We started with SPR spectroscopy using the wild-type LANA *C*-terminal domain (CTD) as ligand and the library compounds at a constant concentration of 500 µM. Compounds that showed a response higher than 9 µ-refractive index units were selected from this screening, which yielded 52 primary binders. (for detailed results see SI, Figure S1). In a second step, we employed DSF experiments as a secondary filter. This assay quantifies a change in thermal denaturation temperature of wild-type LANA *C*-terminal domain by binding

to a compound. Generally, an increase of melting temperature indicates a stabilization of the protein due to binding of a small molecule. Our experiments showed for almost all compounds a decrease in melting temperature for LANA. A decrease of melting temperature may indicate a destabilization of the protein by compound binding. Although usually an increase in protein stability and, thus, increase in melting temperature is observed for target binders, also negative shifts are commonly considered as binding events.[17] As a consequence, we selected 20 compounds, which showed a significant thermal shift $T_M \geq + 0.5$ °C and $T_M \leq -1.0$ °C for further investigations (for detailed results see SI, Figure S2).

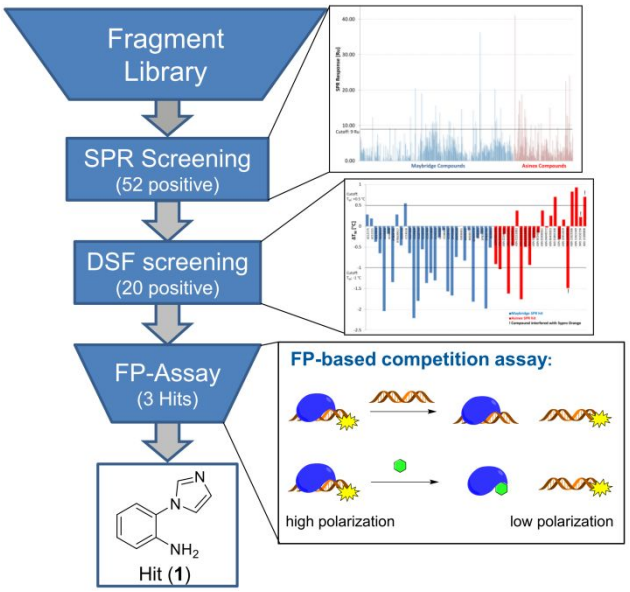

Figure 3. Screening procedure using two different fragment libraries targeting LANA. In total 720 compounds were screened using SPR experiments, followed by DSF. A FP-based assay was used to identify promising interaction inhibitors, which resulted in three promising hits.

Establishment of FP-Assay. For further characterization and optimization, our compounds were tested for inhibition of the DNA-LANA interaction using a fluorescence polarization (FP) -based competition assay. The FP assay is a rapid and quantitative method for identification of small molecular macromolecule-macromolecule interaction inhibitors.[18] For this process we used a mutant of the KSHV LANA *C*-terminal DNA binding domain (DBD) (aa1008-1146) that lacked the ability to form oligomers of LANA DBD dimers.[7] In previous studies it was observed that the wild-type LANA *C*-terminal domain (LANA CTD (aa934-1162)) precipitated readily following the addition of either specific or unspecific DNA.[19] It has the ability to form higher-order oligomers, which contribute to the low solubility in the presence of DNA. For avoiding these solubility problems, multiple point mutations were inserted into the basic patch and the oligomerization interface of LANA DBD; none of these mutations are located at the specific DNA-binding site of LANA, while the basic patch mutations suppress unspecific DNA-binding. This *C*-terminal LANA mutant with the following amino acid mutations: K1055E, K1138S, K1140D, K1141D, R1039Q, R1040Q, A1121E, K1109A, and D1110A shows a high solubility also in presence of oligonucleotides representing the viral LANA-binding sites (LBS) in the viral terminal repeat subunit.[19; 7; 14]

A fluorescence-labeled DNA sequence was employed as competitive binding partner, which corresponds to LANA binding site 2 (LBS2) in a KSHV terminal repeat subunit.[7] We chose LBS2 as the fluorescence probe because of its lower affinity for the LANA DBD and used varying concentrations of unlabeled LBS1, LBS2 and LBS3 to validate and optimize our assay conditions (see SI, Figure S3 and S4). In accordance with previous reports, we obtained a difference in affinity between the LBS sequences.[7]

FP-based Functional Screening. In order to assess the effect of identified screening hits on LANA-DNA-interaction inhibition we tested them in our FP-based assay using LBS2 as fluorescent probe. Due to their high solubility, the compounds could be tested at high concentrations (1 mM or 500 μM), allowing for the identification of even weak inhibitory effects usually observed with fragment-like scaffolds. Each compound was measured in duplicates and in two independent experiments. Three of the 20 tested compounds showed promising results (Table S9, SI). In this paper we will present the hit optimization and validation for hit **1**. Despite its fragment-like size with a molecular weight of only 159.08 g/mol, this compound showed an inhibitory effect of 25 ± 9 % at 1 mM (Figure 3; SPR at 500 μM: 15.69 ± 9.3 RU; DSF at 500 μM: T_M -1.80 ± 1.41 °C). Considering the large interaction site between LANA and its target DNA sequence, this result was promising and encouraged medicinal chemistry optimization of this fragment hit.

The fragment-like structure of hit **1** provided reasonable opportunities for fragment-growing strategies toward generating drug like LANA-DNA inhibitors. Unfortunately, no X-ray or NMR structure was available when starting this hit optimization endeavor. Hence, structure-guided fragment-linking or -merging approaches were not feasible.

Chemistry. The synthesis of Hit **1** was carried out starting from commercially available 2-Iodo nitrobenzene in two steps. Hit **1** and further imidazole derivatives **9-13** were synthesized via an Ullmann-type coupling reaction with a halogen nitrobenzene and the appropriate imidazole.[20] In a second step, the nitro group was reduced with tin(II)chloride to the amine to yield the target compounds **1** and **9-13**.[21] The *N*-acetyl derivative **8** was obtained by acetylation with acetyl anhydride. Furthermore, the 2-methoxyphenyl imidazole (**14)** was synthesized via copper salt catalyzed coupling of imidazole with (2-methoxyphenyl)boronic acid[22] and by cleaving the

methyl group with aqueous HBr, affording the hydroxyl derivative **15**.[23] The synthesis of the benzoic acid derivatives was done by copper catalyzed coupling with the appropriate halo-benzoic acid and 1*H*-imidaziole in a one step reaction (Scheme 1).[24] Generation of 1-azido aniline (**19)** was achieved by copper catalyzed C-H activation of aniline.[25] The azido intermediates (**20**-**24**) were synthesized from the corresponding anilines using standard azidation methods (conc. H_2SO_4 or conc. HCl, $NaNO_2$, NaN_3 in H_2O).[26] Methyl azidobenzoate (**25**) was synthesized by activation with thionyl chloride followed by treatment with methanol.[27] The 1,2,3-triazoles (**26**-**50**) were synthesized using standard copper(I)-catalyzed click reaction conditions. The appropriate alkyne was dissolved in 1:1 *tert*-butanol:water and treated with DIPEA, $CuSO_4 \cdot 5H_2O$ and sodium ascorbate under argon atmosphere, followed by the addition of the corresponding azide. Amino-phenyl-substituted compounds (**51**-**55**) were synthesized from the appropriate amino-phenyl scaffold by treatment with different halogen alkyl analogues under basic conditions in DMF (Scheme 2).

Scheme 1. Synthesis of Hit I and 1*H*-imidazole-1-yl derivatives.[a]

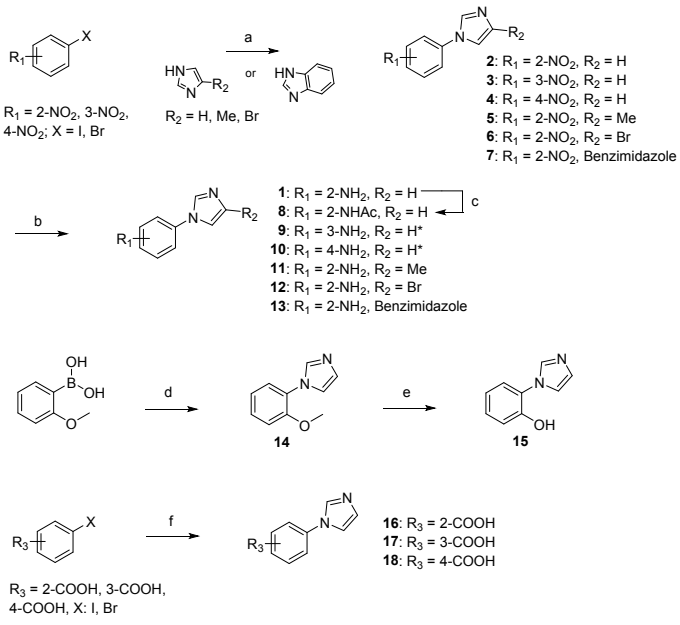

[a]Reagents and conditions: (a) K_3PO_4, CuI abs. DMF, 110 °C, 24 h; (b) $SnCl_2$, EtOH, 80 °C, 30 min; (c) H_2SO_4, AcOH, Ac_2O, rt, 16 h; (d) Imidazole, CuCl, MeOH, 80 °C, 16 h; (e) 48% aq. HBr, 100°C, 16 h; (f) K_2CO_3, CuCl, *N*,*N*′-dimethylmethanediamine, DMF, 120 °C, 24 h.

Scheme 2. Synthesis of azide intermediates and reaction of aryl azides with different alkynes using click chemistry and derivatives.[a]

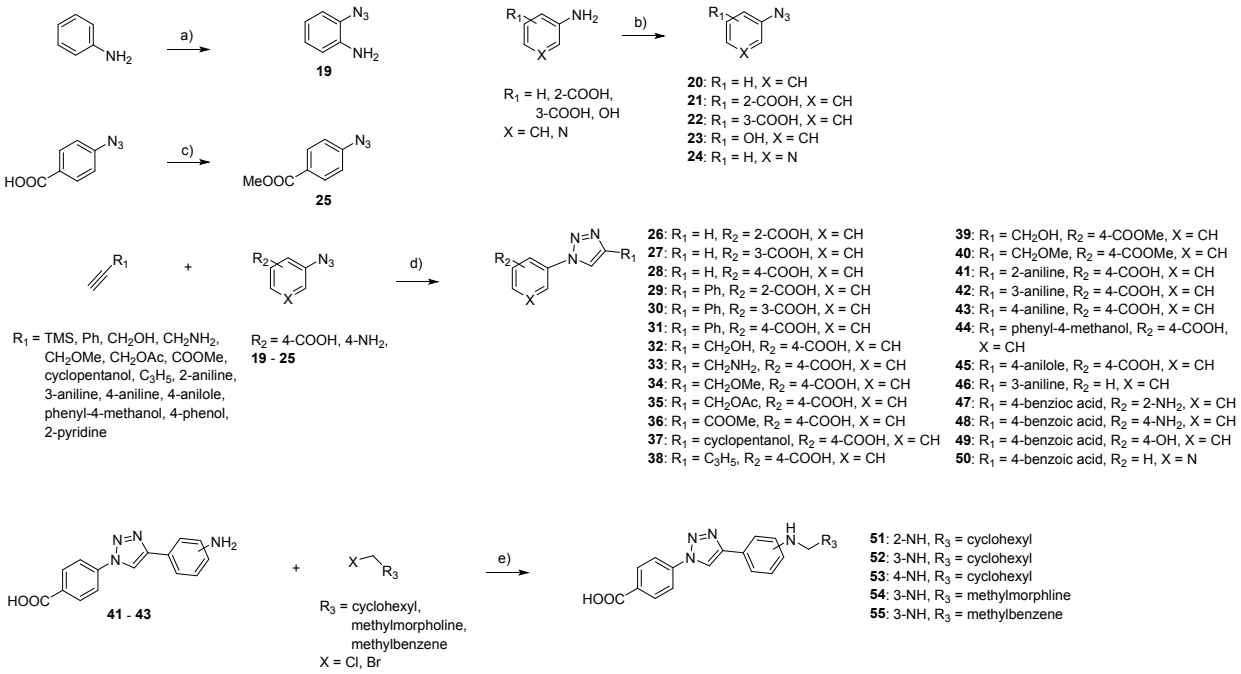

[a]Reagents and conditions: (a) $TMSN_3$, CuBr, TBHP, MeCN, 0 °C → rt, 16 h; (b) conc. H_2SO_4 or conc. HCl, $NaNO_2$, NaN_3, H_2O, 0 °C, 1,5 h; (c) $SOCl_2$, MeOH, 0 °C→ rt, 16 h; (d) $CuSO_4 \cdot 5H_2O$, Na-ascorbate, H_2O:*tert*-BuOH (1:1), DIPEA, rt, 16 h; (e) Cs_2CO_3, DMF, 5h, 90 °C.

Stepwise Hit Optimization and Biological Evaluation. For measuring the inhibitory effect of our compounds, we performed dose-response experiments using constant concentrations of the mutated LANA DBD (aa1008-1146) and fluorescence-labeled LBS2 with varying concentrations of test compound. To exclude false positives through interaction with DNA or via fluorescence quenching, we conducted the dose-dependent experiments with and without addition of LANA.

We did not observe any noticeable assay-interfering effect for any of the compounds. The results obtained with our FP-based interaction inhibition assay are listed in Table 1.

Table 1. Inhibitory activity of 1*H*-imidazole-1-yl derivatives in FP-assay at 1 mM.

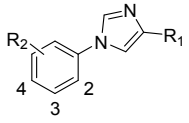

Cpd	R_1	R_2	inhibition [%]@ 1 mM or IC_{50} [µM] (LBS2)
1	H	2-NH_2	25 ± 9 %
11	Me	2-NH_2	91 ± 8 %
12	Br	2-NH_2	13 ± 4 %
13	Benzimidazole	2-NH_2	32 ± 9 %
8	H	2-NHAc	32 ± 16 %
9	H	3-NH_2	n. i.
10	H	4-NH_2	n. i.
2	H	2-NO_2	74 ± 16 %

3	H	3-NO_2	21 ± 16 %
4	H	4-NO_2	22 ± 16 %
14	H	2-OMe	15 ± 12 %
15	H	2-OH	51 ± 13 %
16	H	2-COOH	333 ± 59 μM*
17	H	3-COOH	19 ± 9 %
18	H	4-COOH	13 ± 1 %

*maximum effect was 50 % displacement..

The aim of this first series of derivatives was to identify possible growth vectors to increase size and potency of the compound. Hence, substituents at the imidazole (R1) as well as the phenyl ring (R2) were introduced. Notably, moieties of different size (**11**-**13**) were tolerated at R1. In particular, the methyl derivative **11** showed an improved inhibitory effect of 91 ± 8 % at 1 mM. We concluded that position R1 should be further explored (*vide infra*) as a possible growth vector. Regarding R2, we first varied the position of the amino group at the phenyl ring and investigated the effect of acetylation (compounds **8**-**10**). However, these modifications did not improve the inhibitory effect on the DNA-LANA-interaction significantly. Hence, we introduced different hydrophilic moieties like nitro (**2**-**4**), methoxy (**14**), hydroxyl (**15**) and carboxy (**16**-**18**) groups instead. To our surprise, the presence of a carboxylic acid on the aromatic moiety was tolerated. For compound **16** we were able to plot a full sigmoidal inhibition curve providing an

IC_{50} value of 333 ± 59 µM, with a restriction that the maximum effect leveled out at 50% displacement. Considering the rather basic interaction surface at the DNA-binding domain of LANA, the effectiveness of the acidic moiety in compound **16** was indeed a plausible finding in hindsight. Furthermore, it rendered an unfavorable compound-DNA-interaction as the cause for the observed activity in the FP-assay very unlikely.

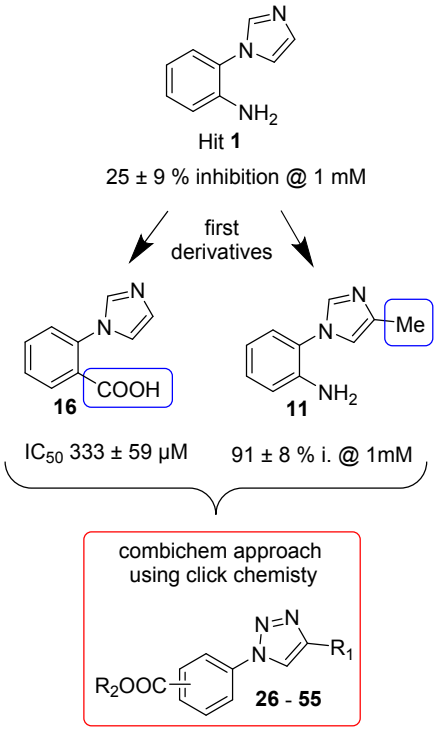

Figure 4. From our initial screening Hit **1** first derivatizations lead to compounds **11** and **16**, which served as a starting point for a combichem approach using click chemistry.

These initial findings inspired us to conduct a combinatorial chemistry approach exploiting the copper(I)-catalyzed alkyne-azide cycloaddition as a straight-forward synthetic method for the

rapid generation of a reasonable number of new derivatives. This prototypic click chemistry provides very efficient and robust reactions under mild conditions and has become a powerful tool in drug discovery.[28] Assuming that the replacement of the imidazole moiety by a triazole core is tolerated, this strategy would dramatically accelerate the establishment of structure-activity-relationships. Further considerations for the design of the click library were the envisioned fragment-growth in the direction of residue R1 (Figure 4) as well as the switch from the amino to the carboxylic group in the western part of the molecule. Hence, we first checked whether this strategy was valid by synthesizing compounds **26-31** (Table 2).

Table 2. Inhibition of first series of 1,2,3-triazole compounds in FP-assay.

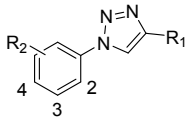

Cpd	R1	R2	IC_{50}(LBS2) [μM] or Inhibition [%]*
26	H	2-COOH	12 ± 10 %
27	H	3-COOH	98 ± 1 %
28	H	4-COOH	35 ± 3 %
29		2-COOH	13 ± 1 %

30		3-COOH	43 ± 17 %
31		4-COOH	232 ± 10 μM

*Inhibition [%] at 1 mM.

Indeed, by comparing the carboxylic acid imidazole compounds (**16-18**) and the carboxylic acid triazole analogs (**26-28**), the introduction of a 1,2,3-triazole was accepted, although the preference for the orientation of the carboxylic acid was shifted from position 2 to 3. This trend even continued when introducing a bulky phenyl moiety in the Eastern part of the molecule (**29-31**). In this case, position 4 was favored for the carboxylic group implying a shift in interaction geometries and/or binding modes between LANA and the inhibitors when moving from imidazolyl to triazolyl to enlarged triazolyl compounds. Derivative **31** showed reasonable potency (IC_{50} value of 232 ± 10 μM) with a significant improvement over inhibitor **16** and additionally provided the opportunity for further modifications replacing the newly introduced bulky phenyl ring. Consequently, we chose this scaffold as the basis for the click library design (Table 3) keeping the carboxylic acid in para position at the aromatic ring in the Western part and varying the substituents on the Eastern side of the molecule.

Table 3. Inhibitory activity of further 1,2,3-triazole derivatives in FP-assay.

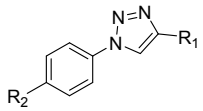

Cpd	R1	R2	IC_{50} (LBS2) [µM]	Cpd	R1	R2	IC_{50} (LBS2) [µM]
32		COOH	79 ± 2	**42**	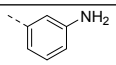	COOH	109 ± 3
33		COOH	30 ± 2	**43**	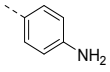	COOH	14 ± 1
34		COOH	210 ± 31	**44**	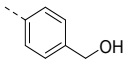	COOH	27 ± 4
35		COOH	n. i.	**45**	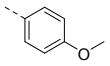	COOH	20 ± 3 % *
36		COOH	163 ± 30	**46**	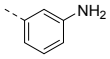	H	n. i.
37		COOH	159 ± 2	**51**	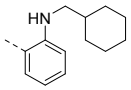	COOH	n. i.
38		COOH	694 ± 41	**52**	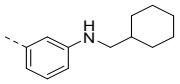	COOH	n. i.
39		COOMe	84 ± 53	**53**	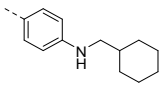	COOH	n. i.

40		COOMe	237 ± 33	**54**	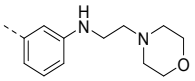	COOH	n. i.
41		COOH	28 ± 1	**55**	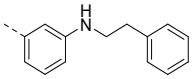	COOH	n. i.

*Inhibition [%] at 500 μM.

A rather general observation when varying the residue R1 was that introducing hydrogenbond-donating groups gave a boost in potency. In detail, direct attachment of a primary hydroxyl or amino group to the triazole core could improve the inhibitory effect by three- to four-fold (**32**: IC_{50} 79 ± 2 μM, **33**: IC_{50} 30 ± 2 μM). A methyl ether (**34**) or methyl ester (**36**), on the other hand, showed just a small potency enhancement compared to compound **29**, while the acetylated analog **35** resulted in a complete loss of activity. Moving from the primary (**32**) to a tertiary alcohol (**37**) by addition of a cyclopentyl motif led to a decrease in activity. However, this derivative shows that obviously bulkier substituents could be tolerated at this position. Also, a rather hydrophobic cyclopropyl residue (**38**) did not yield a potent compound. In parallel, we synthesized two additional compounds with a methyl ester instead of the carboxylic acid at the aromatic ring, **39** and **40**. By comparing compound **32** with **39** and **34** with **40** it seems that also a methyl ester is well accepted, which certainly provides opportunities for future optimization efforts. Additionally, it becomes clear that the beneficial effect of the carboxylic group is not fully relying on a possible ionic interaction with the protein surface. As laid out above, our aim was to explore R1 as a growth vector. Hence, we synthesized aniline derivatives (**41**-**43**). Introducing the amino group in ortho (**41**) or para (**43**) position resulted in the most active compounds to date with IC_{50} values in the low double-digit micromolar range. A loss of activity

was observed with meta aniline (**42**) and para anisole (**45**). Also, the phenyl methanol analog (**44)** showed a rather potent IC_{50} value of 27 ± 4 μM. Keeping the aniline residue and deleting de carboxylic acid at the aromatic region we observed a total loss in activity (**46**). In order to further grow the LANA inhibitor, compounds substituted at the aniline (**51**-**55**) were synthesized. Unfortunately, none of these derivatives were active regardless of the position of the attached substituent. Probably these residues incorporated in **37**-**41** are too bulky and are, thus, not tolerated. Nevertheless, more research should be done in this area of the molecule when moving the project into the lead-generation phase. Finally, we synthesized a series of compounds with an inverted orientation of the 1,2,3-triazole core using 4-ethinyl carboxylic acid and an array of azido benzenes. Compounds **47** and **48** were similar to the previous compounds **41** and **43** showing good IC_{50} values in the same range. Modifying the para aniline analogue to a para phenol (**49**) resulted in slight loss of activity. Besides that, for the 2-pyridine derivative **50** we observed an IC_{50} of 17 ± 1 μM (Table 4)**.**

Table 4. Inhibitory activity of compounds with inverted orientation of the 1,2,3-triazole core in FP-assay.

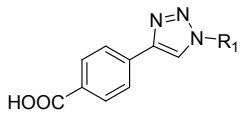

Cpd	R_1	IC_{50} (LBS2) [μM]
47		18 ± 3
48	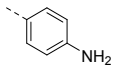	19 ± 1
49	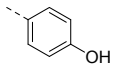	52 ± 3
50		17 ± 1

Qualification of Obtained Optimized Hits.

Comparison of the Inhibition of the Interaction between LANA and LBS1, 2, and 3. In order to investigate whether inhibitors of the LANA-LBS2 interaction would also interfere with protein binding to the other LANA binding sites, we modified our FP assay protocol to also include labeled LBS1 and LBS3 sequences as fluorescent probes. We selected six compounds (**37**, **41**-**43**, **47**, **50**) with differing activity against LBS2 for this assessment and the determined IC_{50} values are summarized in Table 5. Notably, we observed IC_{50} values in a similar rage

compared to the inhibition against LBS2 probe. Additionally, we calculated the logP value and the ligand efficiency (LE) for these compounds to provide a metric for comparing the most potent hits taking potency and molecular weight into account.[29] The logP value is defined as the partition coefficient of a given compound between octanol and water. It provides information about its hydrophobicity and logP values below 3 are found generally in aqueous medium (e.g. blood serum).[30] The LE value is defined as the binding energy of a compound for its target divided by its number of heavy atoms and, hence, it enables to identify those hits, which interact efficiently with most of their atoms. In praxis, an LE of 0.3 or greater is considered to characterize a suitable hit for the optimization to a drug-like compound.[31] Notably, compounds **41**, **43**, **47**, and **50** displayed a LE value of 0.3 or higher and logP values below 3, hence, are suitable scaffolds for further optimization efforts. Considering that these hits have to compete with a macromolecule (DNA) upon binding to a rather flat interaction surface, these results are encouraging.

Table 5. Comparison of IC_{50} values obtained by using LBS1, 2 or 3 as fluorescent probe, clogP and LE.

Cpd	Structure	IC_{50} LBS1	IC_{50} LBS2	IC_{50} LBS3	clogP	LE
37	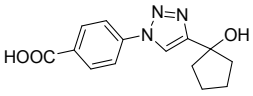	104 ± 33 μM	159 ± 2 μM	39 ± 4 μM	1.80	0.26
42	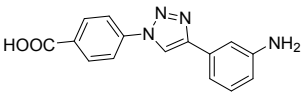	136 ± 27 μM	109 ± 3 μM	106 ± 32 μM	2.78	0.26

41	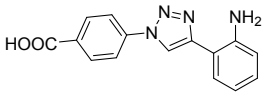	25 ± 1 μM	28 ± 1 μM	26 ± 1 μM	2.78	0.30
43	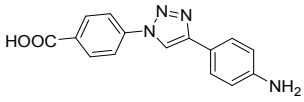	19 ± 55 μM	14 ± 1 μM	12 ± 1 μM	2.78	0.32
47	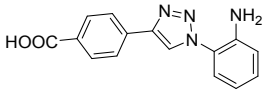	25 ± 1 μM	18 ± 3 μM	26 ± 1 μM	2.78	0.32
50	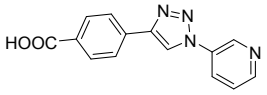	20 ± 3 μM	17 ± 1 μM	19 ± 3 μM	2.00	0.33

EMSA (Electrophoretic Mobility Shift Assay) as Orthogonal Interaction Inhibition Assay.

As an orthogonal interaction inhibition assay, EMSA was used to probe the ability of these six selected compounds to inhibit the DNA-LANA interaction (Figure 5). In this assay, solutions of protein, nucleic acid and inhibitor were combined and the resulting mixtures were subjected to electrophoresis under native conditions.[32] We evaluated the effects of the compounds using fixed concentrations of DNA probes of 20 nM, LANA DBD mutant of 200 nM and compounds of 500 μM. The probes were Dy-682-modified and a purified GST protein was used as a control. We performed the EMSA with two different DNA probes: An oligonucleotide representing only LBS1 for comparing the results with the results of our previous FP assay (Figure 5 A) and a longer oligonucleotide containing both of the LBS1 and LBS2 sequences (Figure 5 B). The latter also forms trimeric complexes with LANA (SI, Fig. S6). In both experiments, we observed that the compounds with IC_{50} values in the triple-digit micromolar range have no specific effect on the DNA-LANA interaction at the concentration used. Importantly, the aniline analog having an IC_{50} value in the lower double-digit micromolar range caused a significant decrease in the intensity of the DNA-LANA complexes and an increase in the intensity of the band representing

the free DNA probe. This clearly indicated that these compounds inhibit the interaction of the LANA DBD mutant with LBS1 and/or LBS1+2.

The most effective inhibitor was the pyridine analogue (**50**, IC_{50} 17 ± 1 μM). The single LBS1 probe (Fig. 5 A) could be displaced almost completely and the combined LBS1-LBS2 probe (Fig. 5 B) to a significant extent. Additionally, we performed further dose-dependent EMSA experiments with the most efficient compound **50** using LBS1 as probe and the LANA DBD mutant as well as wild-type LANA *C*-terminal domain (CTD) (aa934-1162) as protein (for more information see SI, EMSA gels: Figure S9 and S10; calculated IC_{50} values see Figure S11, IC_{50} (LANA DBD mutant) 426 ± 2 μM and IC_{50} (LANA CTD wild-type) 435 ± 6 μM).

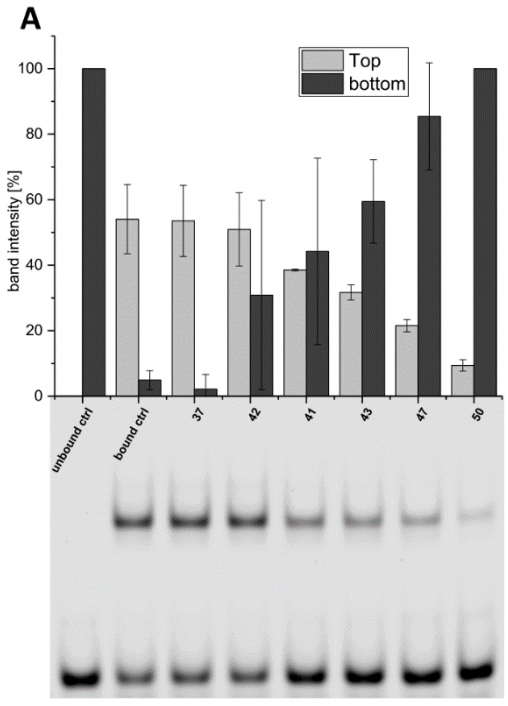

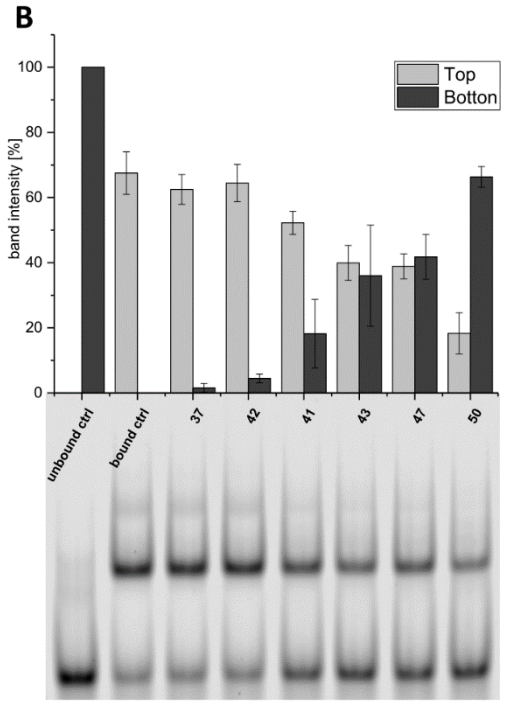

Figure 5. EMSA analysis of compounds **37**, **41**, **42**, **43**, **47**, and **50** using (**A)** LBS1 and (**B**) LBS1+2 as probes. Representative EMSA gels of one independent experiment are shown, respectively, containing: unbound control: GST+LBS1 or LBS1+2, bound control: DMSO+LANA+LBS1 or LBS1+2 and compounds: Cpd+LANA+LBS1 or LBS1+2. Bar graphs are shown with normalized data points (inhibition from 0-100%) representing mean intensities of top band values (LANA-LBS-complex) and bottom band values (single LBS). The experiment was performed in duplicates and the standard deviation given, each compound was used at 500 μM, proteins at 200 nM and DNA probe concentration was 20 nM.

MST and STD NMR Studies for Further Characterization of Ligand Binding. We used MST to quantify the binding affinity of compound **50** to LANA DBD mutant and determined the dissociation constant K_D.[33] The binding assay was performed using the labeled LANA DBD mutant protein at a concentration of 50 nM and starting the dose-response curve with a ligand concentration of 1 mM. The calculated K_D for the binding of compound **50** to LANA was

determined to be 23 ± 1 μM. The detected binding curve is shown in Figure 6, A. We also attempted crystallography of the LANA DBD-inhibitor-complex, but have so far not been successful. With the aim to gather information on the mode of binding, we performed ligand-observed STD NMR studies with compounds **41**, **47** and **50**. The STD NMR can provide information on the putative orientation of a given binder to the target of interest in absence of any structural data of the protein. In this assay, protons that are closest to the protein upon binding, show the strongest STD effect. In our measurement, samples contained a 40-fold excess of compound (1 mM) relative to LANA DBD mutant (25 μM) and were recorded at 298 K (Figure 6, B). The STD effects (I/I_0) were measured and calculated for each proton of the ligand. The STD effect of compound **50** is shown in Figure 6, B. The overlaid spectra were normalized to the signals of H-1 and H-2, which gave the strongest enhancement and, hence, can be assumed to interact the most with the protein surface. These observable variations of the STD effects suggest that the compound binds in a defined orientation to the protein where the pyridine moiety faces the protein surface with its aromatic nitrogen. It can be assumed that this motif acts as a hydrogen bond acceptor. STD effects of H-3 and H-4 (53% and 61% of H-3/H-4, respectively) suggest, that these protons are not in direct contact with the protein and should, be further investigated as potential growth vectors. Indeed, inactive compounds **51**-**55**, were already grown in this direction and lead to abolished activity.

However, the introduced residues were rather large leaving the option of smaller less bulky substituents to be tried. The four protons referred to by H-8 and H-9 presumably divide into two populations: Two hydrogens which are closer to the protein surface and two which are more remote (see Figure 6, B). As these are indistinguishable in the STD NMR experiment, the observed effect should be a mean of the signals from both populations. As a consequence,

growth of the compound breaking this ambiguity is a potential path forward in future optimization efforts.

For compound **41** and **47** we observed similar STD effects (see Figure S12, SI). The protons from the aniline next to the amino group gave the strongest enhancement. This also implies that the NH_2 plays an important role as a hydrogen bond acceptor or donor for binding.

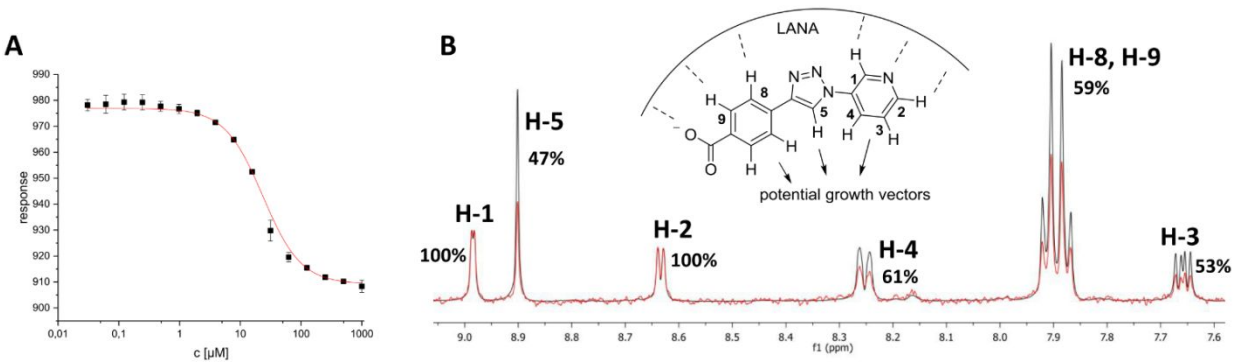

Figure 6. (**A**) Dose-dependent MST interaction curve of compound **50** with LANA DBD mutant. (**B)** STD experiments of compound **50** in complex with LANA DBD mutant. The reference spectrum is displayed in black (STD-off) and STD difference spectra (STD-on) in red. Overlaid spectra were normalized to the signals for H-1 and H-2, which showed the strongest enhancement.

Molecular Docking. In order to generate a possible binding mode of the optimized hit **50** to LANA, we performed docking experiments taking the STD-NMR data into account. Importantly, we specifically searched for target-ligand complex geometries, which are in line with the gathered experimental data. As we demonstrated that this compound binds to LANA (FP assay, MST, STD NMR) and is able to displace the DNA (FP-assay, EMSA), we directed our docking experiment to the DNA-binding site of the target (Figure 7 A). This approach intentionally neglects a possible allosteric mechanism of our compound, which we consider to be rather unlikely due to the rigidity of the DNA-binding domain.

In order to identify the initial docking site, we selected those LANA residues, which were in close proximity (4.5 Å) to the DNA atoms found in PDB entry 4uzb.[7] Docking to this large interaction surface yielded three distinct clusters (Figure 7 A). We searched for a binding pose of

our inhibitor capable of prominently displacing the DNA from the protein. In general, cluster site 2 was located at the center of the LANA-nucleic acid interaction and would enable to disrupt major as well as minor-groove interactions. Sites 1 and 3 were located on the peripheral areas of the LANA-DNA interface. Hence, we selected cluster site 2 for a more focused re-docking experiment and screened the yielded binding poses for compliance with the STD NMR data (see Figure 6 B). We selected the highest scoring pose, which met the criterion of bringing protons 1 and 2 as well as one pair of protons 8 and 9 into close proximity to the protein surface, while exposing protons 3, 4, and 5 as well as the other 8, 9 pair (Figure S13, SIand Figure 6 B). This pose was further refined through local energy minimization and is depicted in Figure 7 B and C. A very prominent interaction partner suggested by this pose is Gln1015. Due to the symmetrical assembly of the LANA dimer, each Gln1015 from either of the two protein chains can contribute to inhibitor binding by acting as hydrogen-bond donors to the carboxyl group. Furthermore, Gln1073 and Val1019 form hydrogen-mediated interactions with the pyridine motif of **50**. As seen from the 2D interaction profile (Figure 7 C), proton at position 2 is detected as 'solvent exposed' although it was in van-der-Waals contact with the protein (see Figure S13, SI). However, this is in agreement with the observation that introduction of an aniline motif is tolerated in this position (**43**). Finally, we postulate a possible cation-π interaction between nearby Lys1069 and the central triazole motif, which would further add to the attractive forces between LANA and the inhibitor. At this point, we would like to stress, that the preferential docking pose is hypothetical and needs further validation through wet lab experiments, for example, via single-amino acid mutation of the strongly interacting Glu1015. Nonetheless, it is in line with currently available data and, hence, a plausible binding mode to base structure-guided modifications on. Next optimization efforts will be directed toward exploration

of the proposed growth vectors (Figure 6 B). The surface of LANA at the DNA binding site is densely covered with possible hydrogen-bonding donors and acceptors, which could be exploited for further attractive interactions.

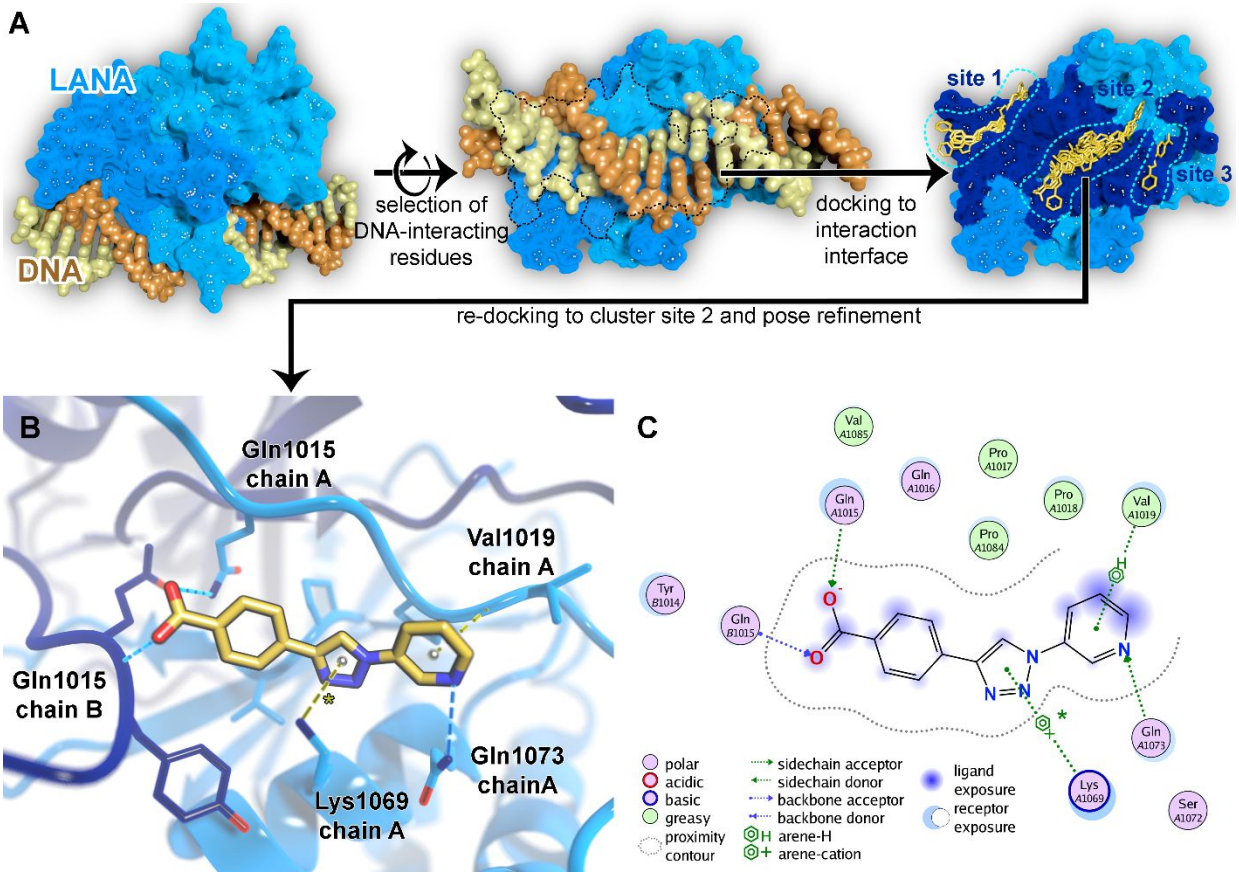

Figure 7. Design (**A**) and result (**B** and **C**) of STD-NMR-informed docking study performed on **50**. (**A**) Docking was conducted using PDB entry 4uzb (left). Residues that make up the docking site were selected based on proximity (4.5 Å) to DNA in complex structure (dashed black line, middle; dark blue surface, right). First docking resulted in three distinct clusters (light blue dashed lines; right). Cluster site 2 was selected for re-docking and subsequent pose refinement. (**B**) 3D and (**C**) 2D representation of the plausible binding pose of **50**. A putative cationπ interaction mediated by Lys1069 is shown and marked with an asterisk.

Conclusion

In this study, we successfully obtained a qualified fragment-sized hit capable of displacing a viral nucleic acid sequence from the DNA-binding domain of the Latency-Associated Nuclear Antigen (LANA) – a potential antiviral drug target to treat Kaposi´s Sarcoma Herpes Virus (KSHV) infections. We achieved this by means of fragment-based drug design employing biophysical screening via SPR and DSF as two orthogonal selection filters followed by functional evaluation through fluorescence polarization (FP). FP also guided hit optimization toward low micromolar activity. Favorable ligand efficiency (> 0.3) and low lipophilicity combined with additional EMSA, MST, and STD NMR experiments corroborating specific target interaction qualify hit **50** as a suitable starting point for a follow-up lead generation campaign. Future optimization efforts will be aided by a wet lab-informed docking pose and amenability of the described scaffold to facilitate CombiChem-driven derivatization via click chemistry. In parallel, continuing efforts are underway to identify a suitable crystallographic system for the generation of protein-ligand complex structures, which would ultimately enable structure-based drug design. The ability to inhibit a nucleic acid-involving macromolecule-macromolecule interaction by a small molecular scaffold is encouraging. The same is true for the promise to break the latent replication cycle of a herpesviral infection. In our opinion, both concepts are challenging, yet worthwhile endeavors.

Experimental Section

Materials and Methods.

All reagent-grade chemicals were obtained from commercial suppliers were used as received. All reactions were carried out under argon atmosphere. Automated column flash chromatography (Combi Flash Rf+ von Teledyne ISCO, Lincoln, NE, USA) was performed on silica gel (Axel Semrau, Sprockhövel Germany) Preparative high pressure liquid chromatography (HPLC, Ultimate 3000 UHPLC+ focused, Thermo Scientific) purification was performed on reverse phase column (C18 column, 5 μm, Macherey-Nagel, Germnay). For gradient eluation a mobile phase consisting of acetonitrile containing 0.05% formic acid (FA) [v/v] and water containing 0.05% FA [v/v] was used. The syntheses were not optimized regarding yields. 1H and 13C NMR were recorded on a Bruker Fourier spectrometers (300/500 or 176/126/75 MHz). Chemical shifts (δ) are reported in parts per million (ppm) relative each reference solvent. The chemical shifts recorded as δ values in ppm units by reference to the hydrogenated residues of deuterated solvent as internal standard. Coupling constants (*J*) are given in Hertz (Hz) and splitting patterns are designated as follows: s, singlet; d, doublet; dd, doublet of doublets; t, triplet; m, multiplet; br. broad signal. Purity of all final compounds was measured on the UV trace recorded at a wavelength of 254 nm and was determined to be > 95 % by reverse phase liquid chromatography mass spectrometer (LCMS). High resolution mass spectra of all final compounds were measured on a Thermo Scientific Q Exactive Focus (Germany) equipped with DIONEX ultimate 3000 UHPLC+ focused and can be found in supporting information.

Procedure I: General synthesis 1-(nitrophenyl)-1*H*-imidazole 2-7. The appropriate halo-nitrobenzene (1 eq.) was dissolved in DMF and treated with K_2CO_3 (1.2 eq.), CuI (0.1 eq.), and substituted 1*H*-imidazole (1.2eq.) or 1*H*-benzoimidazole (1.2 eq.) under argon atmosphere. The mixture was stirred at 120 °C for 24 h. After cooling to room temperature, the solids were filtered off and washed with ethyl acetate (3x). The combined filtrate was concentrated under reduced pressure. The resulting product was purified by column chromatography. Experimental details can be found in supporting information. Compound **2** is presented as an example. 1-(2-nitrophenyl)-1*H*-imidazole **2** was prepared according to general procedure I using 2-iod–nitrobenzene (100 mg, 0.40 mmol), K_2CO_3 (66 mg, 0.48 mmol), CuI (7.5 mg, 0.04 mmol), 1*H*-imidazole (33 mg, 0.48 mmol) and DMF (3 mL). The obtained crude was purified by column chromatography (PE:EE 1:9) to yield the title compound (36 mg, 0.19 mmol, 49 %). ^{1}H NMR (300 MHz, $CDCl_3$) δ ppm 7.10 (s., 1 H) 7.25 (s., 1 H) 7.48 (dd, *J* = 7.82, 1.21 Hz, 1 H) 7.57-7.71 (m, 2 H) 7.71-7.79 (m, 1 H) 8.01 (dd, *J* = 8.06, 1.35 Hz, 1 H); ^{13}C NMR (75 MHz, $CDCl_3$) δ ppm 125.35, 128.65, 129.62, 130.66, 133.70, 137.23.

Procedure II: General synthesis of (1*H*-imidazol-1-yl)anilines 1, 9-13. 1-(nitrophenyl)-1*H*-imidazole derivatives (1 eq.) were dissolved in ethanol and treated with tin(II)chloride (5 eq.). The mixture was refluxed for 30 min and after cooling to room temperature the solids were filtered off and washed with ethanol. The filtrate was combined and solvent was removed under reduced pressure. The crude was dissolved in ethyl acetate and extracted with saturated $NaHCO_3$ solution. The combined organic layers were dried over sodium sulfate and concentrated under reduced pressure. The products were purified by flash chromatography or by reverse-phase HPLC and were dried at a lyophilisator. Experimental details can be found in the supporting information. Compound **1** is presented as example. 2-(1*H*-imidazol-1-yl)aniline **1** was prepared

to the general procedure II using 1-(2-nitrophenyl)-1*H*-imidazole **2** (150 mg, 0.79 mmol), $SnCl_2$ (890 mg, 3.96 mmol) and ethanol (20 mL). The obtained crude was purified by flash column chromatography (gradient elution, DCM:MeOH 95:5-90:10) to yield the target compound (108 mg, 0.67 mmol, 68%). ^{1}H NMR (300 MHz, $CDCl_3$) δ ppm 3.80 (br. s., 2 H) 6.91-7.02 (m, 2 H) 7.20-7.31 (m, 2 H) 7.34-7.43 (m, 2 H) 7.79 (s, 1 H); ^{13}C NMR (75 MHz, $CDCl_3$) δ ppm 116.35, 118.54, 120.09, 123.25, 127.11, 129.79, 129.92, 137.64, 141.90.

***N*-(2-(1*H*-Imidazol-1-yl)phenyl)acetamide (8).** 2-(1*H*-imidazol-1-yl)aniline **1** (50 mg, 0.31 mmol) was dissolved in a mixture of acetic acid (4 mL) and acetic acid anhydride (2 mL). 1 drop sulfuric acid was added and stirred at room temperature for 16 h. The reaction mixture was neutralized with aq. 10% NaOH solution and extracted with DCM (2x). The combined organic phases were dried over sodium sulfate and concentrated under reduced pressure to give the crude which was purified by HPLC (revered-phase, mobile phase consisting of acetonitrile containing 0.05% FA [v/v] and water containing 0.05% FA [v/v], gradient elution: 5:95-60:40) to yield the target compound (8 mg, 0.04 mmol, 13%). ^{1}H NMR (300 MHz, $CDCl_3$) δ ppm 2.12 (s, 3 H) 7.06-7.11 (m, 1 H) 7.19 (d, J = 1.02 Hz, 1 H) 7.23 (s., 1 H) 7.24 (s, 1 H) 7.43-7.51 (m, 1 H) 7.51-7.54 (m, 1 H) 7.74 (s., 1 H) 8.25 (d, J = 8.20 Hz, 1 H); ^{13}C NMR (75 MHz, $CDCl_3$) δ ppm 24.28, 120.20, 123.78, 124.99, 126.79, 129.83, 130.30, 133.36, 137.63, 168.90.

1-(2-Methoxyphenyl)-1*H*-imidazole (14). (2-methoxyphenyl)boronic acid (150 mg, 0.98 mmol), 1*H*-Imidazole (80 mg, 1.18 mmol) and CuCl (5 mg, 0.05 mmol, 5 mol%) were dissolved in methanol (10 mL) and refluxed for 16 h. After cooling to room temperature the solvent was removed under reduced pressure, the obtained crude dissolved in ethyl acetate and extracted with water. The combined organic phases were dried over sodium sulfate and concentrated under reduced pressure to give the crude. The crude was purified by column chromatography

(DCM:MeOH 95:5) to yield the title compound (70 mg, 0.40 mmol, 41%). ^{1}H NMR (300 MHz, methanol-d_4) δ ppm 3.87 (s, 3 H) 7.01-7.13 (m, 2 H) 7.22 (d, *J* = 8.29 Hz, 1 H) 7.30-7.48 (m, 3 H) 7.88 (s, 1 H); ^{13}C NMR (75 MHz, methanol-d_4) δ ppm 56.58, 113.90, 122.15, 122.30, 126.91, 127.62, 128.75, 130.77, 139.18, 154.33.

2-(1*H*-Imidazol-1-yl)phenol (15). 1-(2-methoxyphenyl)-1*H*-imidazole **14** (50 mg, 0.28 mmol) was dissolved in 48% hydro bromic acid in water (6 mL) and refluxed for 16 h. The mixture was neutralized with saturated $NaHCO_3$ solution and extracted with ethyl acetate (2x). The combined organic phases were dried over sodium sulfate and concentrated under reduced pressure to give the crude, which was purified by column chromatography (DCM:MeOH 95:5) to yield the title compound (40 mg, 0.25 mmol, 90%). ^{1}H NMR (300 MHz, DMSO-d_6) δ ppm 6.91 (td, *J* = 7.59, 1.40 Hz, 1 H) 6.98-7.11 (m, 2 H) 7.16-7.26 (m, 1 H) 7.33 (dd, *J* = 7.87, 1.63 Hz, 1 H) 7.45 (s., 1 H) 7.94 (s., 1 H) 10.27 (br. s., 1 H); ^{13}C NMR (75 MHz, DMSO-d_6) δ ppm 116.90, 119.54, 124.75, 125.25, 128.47, 150.23.

Procedure III: General procedure of (1*H*-imidazol-1-yl)benzoic acids 16-18. The appropriate hal-benzoic acid (1 eq.) was dissolved in DMF (0.1 M) and treated with *N*1,*N*2-dimethylethane-1,2-diamine (0.2 eq.), K_2CO_3 (2.2 eq.), CuCl (0.1 eq.), and 1*H*-Imidazole (1.5 eq.) under argon atmosphere. The mixture was stirred at 120 °C for 24 h. After cooling to room temperature the solids were filtered off and washed with ethyl acetate. The combined filtrate was concentrated under reduced pressure. The resulting product was purified using prep. HPLC (revered-phase, mobile phase consisting of acetonitrile containing 0.05% FA [v/v] and water containing 0.05% FA [v/v]; gradient elution, 5:95-90:10) to yield the target compound. Experimental details can be found in supporting information. Compound **16** is presented as example. 2-(1*H*-imidazol-1-yl)benzoic acid **16** was prepared according to general procedure III using 2-iodo–benzoic acid,

*N*1,*N*2-dimethylethane-1,2-diamine, K_2CO_3, CuCl, 1*H*-imidazole and DMF. ^{1}H NMR (500 MHz, DMSO-d_6) δ ppm 7.40 (br. s., 1 H) 7.57 (br. s., 1 H) 7.59-7.72 (m, 2 H) 7.72-7.84 (m, 1 H) 7.99 (br. s., 1 H) 8.51 (br. s., 1 H); ^{13}C NMR (126 MHz, DMSO-d_6) δ ppm 119.23, 120.21, 123.52, 126.37, 127.64, 130.14, 130.25, 135.58, 138.45, 166.53.

2-Azidoaniline (19). Aniline (500 mg, 5.4 mmol) was dissolved in acetonitrile (100 mL). *Tert*-butylhydroperoxide (1.5 mL, 8.1 mmol) and copper(I)bromide (77 mg, 0.5 mmol) were added and the mixture was cooled to 0 °C. At 0 °C $TMSN_3$ (1.4 mL, 10.7 mmol) was added dropwise and the reaction mixture was stirred at room temperature overnight. The solvent was removed under reduced pressure and the crude product purified by flash chromatography (PE:EE, gradient elution, 1:0-9:1) to yield the target compound (230 mg 1.72 mmol, 32%). ^{1}H NMR (300 MHz, $CDCl_3$) δ ppm 7.05 (d, 1 H, *J* = 9 Hz), 6.97 (dd, 1 H, *J* = 7,5 Hz), 6.80 (dd, 1 H, *J* = 7,5 Hz), 6.71 (d, 1 H, *J* = 3 Hz), 3.81 (br. s., 2 H); ^{13}C NMR (75 MHz, $CDCl_3$): δ ppm 138.1, 125.6, 125.2, 119.1, 118.3, 115.8.

Azido benzene (20). Aniline (364 mg, 4.0 mmol) was dissolved in ethyl acetate (8 mL), cooled to 0 °C and water (1 mL) and conc. HCl (2.4 mL) were added. Sodium nitrit (469 mg, 6.8 mmol, 1.7 eq.) dissolved in water (1 mL) was added slowly. The reaction mixture was stirred for 30 min at 0°C. Subsequently, sodium azid (442 mg, 6.8 mmol, 1.7 eq.) in water (1 mL) was added slowly at 0 °C. After stirring at room temperature for 1.5 h, the TLC indicated full conversion and the mixture was neutralized and extracted with ethyl acetate (2x). The combined organic phases were dried over sodium sulfate and concentrated under reduced pressure to give the crude. The crude product (300 mg) was used as obtained in the next step without further purifications.

2-Azidobenzoic acid (21). Anthranilic acid (300 mg, 2.2 mmol) were dissolved a mixture of water (10 mL) and sulfonic acid (2 mL) and cooled to 0 °C. Sodium nitrit (151 mg, 2.2 mmol) dissolved in water (1 mL) and added dropwise. The reaction mixture was stirred for 15 min at 0°C. Subsequently, sodium azid (172 mg, 2.6 mmol) in water (1 mL) was added slowly at 0 °C. After stirring at room temperature for 2 h, the TLC indicated full conversion and the mixture was diluted with water and extracted with ethyl acetate (2x). The combined organic phases were dried over sodium sulfate and concentrated under reduced pressure to give the crude. The crude product (250 mg) was used as obtained in the next step without further purifications. MS (ESI-) m/z 162 (M-H)

3-Azidobenzoic acid (22). 3-aminobenzoic acid (300 mg, 2.2 mmol) was dissolved in a mixture of water (10 mL) and sulfonic acid (2 mL) and cooled to 0 °C. Sodium nitrit (151 mg, 2.2 mmol) was dissolved in water (1 mL) and added dropwise. The reaction mixture was stirred for 15 min at 0°C. Subsequently, sodium azide (172 mg, 2.6 mmol) in water (1 mL) was added slowly at 0 °C. After stirring at room temperature for 2 h, the TLC indicated full conversion and the mixture was diluted with water and extracted with ethyl acetate. The combined organic phases were dried over sodium sulfate and concentrated under reduced pressure to give the crude. The crude product (220 mg) was used as obtained in the next step without further purifications. MS (ESI-) m/z 162 (M-H)

4-Azido phenol (23). 4-aminophenol (436 mg, 4.0 mmol) was dissolved in 6 M HCl (15 mL). Sodium nitrit (469 mg, 6.8 mmol, 1.7 eq.) was dissolved in water (3 mL) and added. The reaction mixture was stirred for 30 min at 0 °C. Subsequently, sodium azide (442 mg, 6.8 mmol, 1.7 eq.) in water (1 mL) was added slowly at 0 °C. After stirring at room temperature for 1.5 h, the TLC indicated full conversion and the mixture was neutralized and extracted with ethyl

acetate (2x). The combined organic phases were dried over sodium sulfate and concentrated under reduced pressure to give the crude. The crude product (290 mg) was used as obtained in the next step without further purifications.

3-Azido pyridine (24). 3-Aminopyridine (376 mg, 4.0 mmol) was dissolved in ethyl acetate (8 mL), cooled to 0 °C, water (1 mL) and conc. HCl (2.4 mL) were added. Sodium nitrit (469 mg, 6.8 mmol, 1.7 eq.) dissolved in water (1 mL) was added dropwise. The reaction mixture was stirred for 30 min at 0°C. Subsequently, sodium azide (442 mg, 6.8 mmol, 1.7 eq.) in water (1 mL) was added slowly at 0 °C. After stirring at room temperature for 1.5 h, the TLC indicated full conversion and the mixture was basified with saturated Na2CO3 solution (pH 10) and extracted with ethyl acetate (2x). The combined organic phases were dried over sodium sulfate and concentrated under reduced pressure to give the crude. The crude product (280 mg) was used as obtained in the next step without further purifications.

Methyl 4-azidobenzoate (25). 4-azido benzoic acid (300 mg, 1.8 mmol) were dissolved in methanol (10 mL) and cooled to 0 °C. Thionyl chloride (297 µl, 4.14 mmol) was added dropwise at 0 °C and the reaction mixture was stirred at room temperature overnight. The solvent was removed and the obtained crude was purified by flash chromatography (PE:EE, gradient elution, 1:0-95:5) to yield the product (305 mg, 1.7 mmol, 94%). MS (ESI+) m/z 178 (M+H)

Procedure IV: General synthetic procedure for (1*H*-1,2,3-triazol-1-yl)benzoic acids 26-28. Ethynyltrimethyl silane (1.0 eq.) was suspended in 1:1 mixture of water and methanol under argon atmosphere. Copper sulfate hepta-hydrate (0.5 eq.) and sodium ascorbate (0.5 eq.) were added. After addition of the corresponding azide (1.0 eq.) the mixture was stirred 24 h at room temperature. After full conversion (TLC control) the mixture was acidified with 1 M HCl for

cleaving the TMS group and extracted with dichloromethane (2x). The combined organic phases were dried over sodium sulfate and concentrated under reduced pressure to give the crude. The crude product was purified using preparative HPLC (revered-phase, mobile phase consisting of acetonitrile containing 0.05% FA [v/v] and water containing 0.05% FA [v/v]; gradient elution, 5:95-90:10) and dried on a lyophilizer to yield the target compound. Experimental details can be found in the supporting information. Compound **26** is presented as example. 2-(1*H*-1,2,3-triazol-1-yl)benzoic acid **26** was synthesized according to procedure IV using 2-azidobenzoic acid and ethynyltrimethylsilane as starting material. ^{1}H NMR (500 MHz, DMSO-d_6) δ ppm 7.60 (s., 1 H) 7.63-7.70 (m, 1 H) 7.73-7.79 (m, 1 H) 7.91 (d, J = 8.70 Hz, 2 H) 8.51 (s., 1 H); ^{13}C NMR (126 MHz, DMSO-d_6) δ ppm 126.47, 126.53, 129.84, 130.38, 132.29, 133.35, 135.36, 166.62.

Procedure V: General Synthetic Procedure for Synthesis of copper catalyzed click reaction of alkynes and azides, compounds 29-50. Under argon atmosphere the appropriate alkyne (1.0 eq.) was suspended in 1:1 mixture of water and tert-butanol. DIPEA (2.0 eq.), copper sulfate heptahydrate (0.5 eq-) and sodium-ascorbate (0.5 eq.) were added. After addition of the corresponding azide (1.0 eq.) the mixture was stirred 16 h at room temperature. After full conversion (TLC control) the mixture was acidified with 1 M HCl and the product precipitated. The solids were collected, washed with water and dried under vacuum to obtain the crude product. The products were purified by preparative HPLC (revered-phase, mobile phase consisting of acetonitrile containing 0.05% FA [v/v] and water containing 0.05% FA [v/v]; gradient elution, 5:95-90:10) and dried on a lyophilizer. The reactions and purification steps was not optimized regarding yields. Experimental details can be found in the supporting information. Compound **31** is presented as an example. 4-(4-phenyl-1*H*-1,2,3-triazol-1-yl)benzoic acid **31** was synthesized according to procedure V using 4-azidobenzoic acid and ethynyl benzene as starting

material. ^{1}H NMR (300 MHz, DMSO-d_6) δ ppm 7.39 (dd, *J* = 7.39 Hz, *J* = 7.39 Hz, 1 H) 7.50 (dd, *J* = 7.50 Hz, *J* = 7.50 Hz, 2 H) 7.95 (d, *J* = 7.45 Hz, 2 H) 8.16 (s., 3 H) 9.41 (s, 1 H); ^{13}C NMR (75 MHz, DMSO-d_6) δ ppm 119.65, 125.37, 128.38, 129.01, 129.99, 139.46, 147.56, 167.52.

Procedure VI: General procedure for 4-(4-((cyclohexylmethyl)amino)phenyl)-1H-1,2,3-triazol-1-yl)benzoic acid 51-53. The appropriate 4-(4-(aminophenyl)-1*H*-1,2,3-triazol-1-yl)benzoic acid (30 mg, 0.11 mmol, 1 eq.), cesium carbonate (107 mg, 0.33 mmol, 3 eq.) and (bromomethyl) cyclohexane (39 mg, 0.22 mmol, 2 eq.) were dissolved in DMF (5 mL) and stirred at 90 °C for 5 h. After cooling to room temperature 1 M HCl was added and extracted with DCM (2x). The combined organic phases were dried over sodium sulfate and concentrated under reduced pressure to give the crude. Purification was done by flash column chromatography (DCM:MeOH, gradient elution, 95:5-90:10) to yield the target compound. Experimental details can be found in the supporting information. Compound **51** is presented as example and was obtained with 72% (29 mg, 0.08 mmol) yield. ^{1}H NMR (500 MHz, $CDCl_3$) δ ppm 1.03-1.16 (m, 2 H) 1.19-1.35 (m, 4 H) 1.73 (d, *J* = 12.05 Hz, 1 H) 1.77-1.83 (m, 2 H) 1.83-1.90 (m, 2 H) 4.20 (d, *J* = 6.26 Hz, 2 H) 5.48 (br. s., 1 H) 6.73-6.86 (m, 2 H) 7.15-7.23 (m, 1 H) 7.46 (dd, *J* = 7.71, 1.30 Hz, 1 H) 7.92 (d, J = 8.54 Hz, 2 H) 8.18-8.33 (m, 3 H); ^{13}C NMR (126 MHz, $CDCl_3$) δ ppm 25.68, 26.35, 29.76, 34.68, 37.24, 70.54, 112.96, 116.93, 117.54, 117.56, 119.99, 127.89, 129.59, 130.78, 131.36, 139.93, 145.30, 149.43, 165.47.

4-(4-(3-((2-Morpholinoethyl)amino)phenyl)-1*H*-1,2,3-triazol-1-yl)benzoic acid (54). 4-(4-(3-aminophenyl)-1*H*-1,2,3-triazol-1-yl)benzoic acid **42** (30 mg, 0.11 mmol, 1 eq.), cesium carbonate (107 mg, 0.33 mmol, 3 eq.) and 4-(2-chloroethyl) morpholine (331 mg, 0.22 mmol, 2 eq.) were dissolved in DMF (5 mL) and stirred at 90 °C for 5 h. After cooling to room

temperature the solvent was removed under reduced pressure and purified by flash column chromatography (DCM:MeOH, gradient elution, 95:5-90:10) to yield the target compound (16 mg, 0.04 mmol, 36%) ^{1}H NMR (500 MHz, $CDCl_3$) δ ppm 2.57-2.63 (m, 4 H) 2.81 (t, *J* = 5.87 Hz, 2 H) 3.72-3.76 (m, 5 H) 3.81 (br. s., 2 H) 4.52 (t, *J* = 5.87 Hz, 2 H) 6.72 (dt, *J* = 7.52, 1.74 Hz, 1 H) 7.21-7.26 (m, 2 H) 7.36 (s, 1 H) 7.92 (d, *J* = 8.54 Hz, 2 H) 8.22 (s, 2 H) 8.24 (s, 1 H); ^{13}C NMR (126 MHz, $CDCl_3$) δ ppm 53.88, 57.08, 62.69, 66.97, 112.36, 115.38, 116.15, 117.24, 119.85, 129.93, 130.20, 130.77, 131.39, 140.17, 147.00, 148.94, 165.32.

4-(4-(3-(Phenethylamino)phenyl)-1*H*-1,2,3-triazol-1-yl)benzoic acid (55). 4-(4-(3-aminophenyl)-1*H*-1,2,3-triazol-1-yl)benzoic acid **42** (30 mg, 0.11 mmol), cesium carbonate (107 mg, 0.33 mmol, 3 eq.) and (2-bromoethyl)benzene (41 mg, 0.22 mmol, 2 eq.) were dissolved in DMF (5 mL) and stirred at 90 °C for 5 h. After cooling to room temperature 1 M HCl was added and extracted with DCM (2x). The combined organic phases were dried over sodium sulfate and concentrated under reduced pressure to give the crude. Purification was done by flash column chromatography (DCM:MeOH, gradient elution, 95:5-90:10) to yield the target compound (20 mg, 0.05 mmol, 45%). ^{1}H NMR (500 MHz, $CDCl_3$) δ ppm 3.13 (t, *J* = 6.94 Hz, 2 H) 3.81 (br. s., 1 H) 4.59 (t, *J* = 6.94 Hz, 2 H) 6.72 (d, *J* = 7.63 Hz, 1 H) 7.21-7.26 (m, 2 H) 7.28-7.33 (m, 3 H) 7.35 (d, *J* = 7.63 Hz, 3 H) 7.89-7.92 (m, 2 H) 8.18-8.21 (m, 2 H) 8.22 (s, 1 H); ^{13}C NMR (126 MHz, $CDCl_3$) δ ppm 35.19, 65.86, 112.36, 115.36, 116.14, 117.26, 119.81, 126.70, 128.57, 128.60, 128.90, 128.94, 129.91, 130.29, 130.78, 131.33, 131.36, 137.67, 140.10, 147.00, 148.90, 165.32.

Expression and Purification of His-tagged oligomerization-deficient mutant of the KSHV LANA *C*-terminal DNA binding domain (DBD; aa1008-1146). For the expression of KSHV His-tagged oligomerization-deficient LANA DBD (aa1008-1146) protein pETRO1.01 vector

BL21 (DE3) cells were used.[7] His-tagged LANA DBD target protein was purified by Ni-NTA affinity chromatography (HisTrap HP column) using ÄKTAExpress (GE Healthcare). For more details see SI.

Screening Library. The screening library contained 220 diversity fragment compounds from Asinex (Winston-Slalem, NC, USA) and 500 from Maybrige (Loughborough, UK). The compounds possessing a molecular weight (MW) from 142 g/mol to 398 g/mol and were dissolved in DMSO to 10 mM or 20 mM stocks.

Surface Plasmon Resonance (SPR) Screening. SPR experiments were performed in running buffer (10 mM PBS, pH = 7.4, 5% DMSO [v/v], 0.05% Tween20 [v/v]) using Reichert SR7500 biosensor (Buffalo, NY, USA) with research-grade CMD-500M sensor chips provided by XanTecBioanalytica (Düsseldorf, Germany) at 18 °C. All experiments were performed in two independent experiments. Scrubber 2 software (Version 2.0c 2008, BioLogic Software) was used for processing and analyzing the data. Changes in refractive index due to DMSO-dependent solvent effects were corrected by using a calibration curve (seven solutions, 4.75-5.75% DMSO in buffer).

We immobilized the wild-type LANA *C*-terminal domain (LANA CTD (aa934-1162)), expressed as a His-tagged protein on CMD500 sensor chips using standard amine coupling with ddH2O as immobilization buffer at 25 °C. The carboxymethyl dextran surface was first prepared with sodium borate (1 M, pH 9.5) (5 injections) and was activated with a 7-min injection of a 1:1 ratio of 0.4 M 1-ethyl-3-(3-dimethylaminopropyl) carbodiimide hydrochloride (EDC):0.1 M *N*-hydroxy succinimide (NHS). His-tagged LANA DBD was diluted into sodium acetate (10 mM,

pH 4.5) to 10 mM solution and coupled to the surface with a 1.5 min injection. Remaining activated groups were blocked with a 7-min injection of 1 M ethanolamine (pH 8.5).

Binding experiments were performed at a constant flow rate of 20 µl/min and before starting the experiments 12 warm-up blank injections were done. Zero-buffer blank injections were included for referencing. For SPR screening, all compounds were tested at 500 µM. Each sample was injected twice on two different sensor chips. To collect the binding response the sample was dissolved in running buffer and injected for 120 s association and 300 s dissociation. Compounds which showed a response higher than 9 RU were selected from the first screening (52 compounds). Results are shown in Figure S1, SI.

Differential Scanning Fluorimetry (DSF) Screening. DSF experiments were performed in running buffer (10 mM PBS, pH = 7.4, 5% DMSO [v/v], 0.05% Tween20 [v/v]) using StepOne Plus Real Time PCR System® (Biosystem, Life Technologies Corporation), StepOne Software (StepOne and StepOne Plus Real Time PCR System Version 2.3) as collecting data software and Applied Biosystem® (Protein Thermal Shift Software Version 1.1) as analyzing software. Final concentrations of 20 µM wild-type LANA *C*-terminal domain (LANA CTD (aa934-1162)) and 500 µM of compounds were used. The 52 positives compounds from SPR screening were tested. Compounds showing $T_M > + 0.5$ °C and $T_M < -1$ °C were selected for further investigations. Results are shown in Figure S2, SI.

Fluorescence Polarization (FP) Assay. FP was recorded in black 384-well microtiter plates (Greiner BioOne, catalog number 781900) using CLARIOstar microplate reader (BMG LABTECH, Ortenberg, Germany) with an extinction filter at 485 nm and emission filter at 520 nm. Gain adjustment was performed before starting each measurement to achieve maximum

sensitivity. The FP values were measured in millipolarization units (mP). The experiments were performed in two independent experiments and each sample was tested in duplicates. In all experiments inhibitor and His-tagged oligomerization-deficient LANA DBD (aa1008-1146) mutant (final concentration 200 nM) were pre-incubated for 60 min. After addition of fluorescent labelled DNA (LBS1_flc, LBS2_flc or LBS3_flc, final concentration 10 nM) the samples were incubated for 90 min. Assay was performed in FP-Buffer (10 mM HEPES, 150 mM NaCl, 0.005% [v/v] Tween20, DEPC water) with 5 % DMSO. Assay optimization studies can be found in SI, Figure S3.

Microscale Thermophoresis (MST). According to the MST (nanotemper-technologies.com) guided procedure His-tagged oligomerization-deficient LANA DBD (aa1008-1146) mutant was labeled using the Monolith NTTM His-Tag Labeling Kit RED-tris NTA. The binding assay was performed as described in the MST guided procedure and MST-Buffer (10 mM HEPES, 150 mM NaCl, 2 mM DTT, 0.005% [v/v] Tween20, DEPC water) with 5 % DMSO was used.

Electrophoretic Mobility Shift Assay (EMSA). The EMSA was carried out with slight modifications as described in Hellert *et al*. (2013)[14]. His-tagged oligomerization-deficient LANA DBD (aa1008-1146) mutant protein (200 nM final) was incubated with the compounds (500 µM final) for 1h at RT in the dark in a reaction volume of 15 µL. The reaction buffer consisted of 30 mM Tris HCl pH 7.5, 50 mM KCl, 10 mM MgCl2, 1 mM DTT, 1 mM EDTA, 10% glycerol, 0.25% Tween20, 0.5 mg/mL BSA and 0.05 mg/mL poly(dI-dC). After the initial incubation period the 5´-Dy682-labeled double stranded DNA probe (IBA Lifesciences) (20 nM final) was added to the reaction and incubated for another 30 minutes at RT in the dark. 10 µL of the reaction was run on a pre-run native 5% acrylamide gel for 45 minutes at 100V with tris-borate-

EDTA buffer. Images of the gels were acquired with the Odyssey (Licor) using the Image Studio software. Raw data can be found in SI, Figure S7 and S8.

Saturation-transfer difference (STD) NMR. The STD experiments were recorded at 298 K on a Bruker Fourier spectrometers (500 MHz). The Samples contained a 40-fold excess of compound (1 mM final) relative to *C*-terminal His-tagged oligomerization-deficient LANA DBD (aa1008-1146) mutant (25 μM final). The control spectra were recorded under same conditions containing free compound to test for artefacts. The STD buffer considered 20 mM Bis-Tris-Cl, 300 mM NaCl, 2 mM DTT, pH 6.5 in D_2O containing 5% deuterated DMSO-d_6. The experiments were recorded with a carrier set at 0 ppm for the on-resonance and -40 ppm for the off-resonance irradiation. Selective protein saturation was carried out at 2 s by using a train of 50 ms Gauss-shaped pulses, each separated by a 1 ms delay. The difference in intensity due to saturation transfer was quantified using $STD_{effect} = (I_0-I_{sat})/I_0$ and constitutes an indication of binding. I_{sat} is the intensity of a signal in the on-resonance NMR spectrum, I_0 is the intensity of one signal in the off-resonance or reference NMR spectrum.

Molecular docking. All docking experiments were performed with MOE 2018.01 (Molecular Operating Environment, Chemical Computing Group)[34] while graphic processing for manuscript figures was done using YASARA structure (YASARA Biosciences GmBH)[35] and POV-Ray 3.7.0. First, 4uzb was loaded into MOE. LANA residues in 4.5 Å proximity to DNA atoms were selected and used as initial docking site. Then compound **50** was docked in its deprotonated form to this site ignoring solvent, using 'Triangle Matcher' as placement method and 'London dG' as scoring function with 300. Refinement was done using the 'Induced Fit' method and 'GBVI/WSA dG' scoring function with 50 poses. Amber10:EHT was used as force field. For the re-docking experiment we used the 14 ligand poses found in cluster 2 as docking site ignoring

solvent, using 'Triangle Matcher' as placement method and 'London dG' as scoring function with 100. Refinement was done using the 'Induced Fit' method and 'GBVI/WSA dG' scoring function with 10 poses. Amber10:EHT was used as force field. The proposed binding pose depicted in Figure 7 was selected from the resulting array of poses based on the following criteria: 1) compliance to STD-NMR data (see also Figure S12) 2) docking score and 3) number of occurrence. The highest score of the selected pose was position 35 and it occurred eight times within the 140 generated poses. Refinement of the selected pose was done using the built-in 'QuickPrep' function with standard parameters and the Amber10:EHT force field.

ASSOCIATED CONTENT

Supporting Information (SI)

Synthetic procedures and characterizations of compounds **3**-**7**, **11**-**13**, **17**, **18**, **27**-**30**, **32**-**50**, **52** and **53**, high resolution mass spectra of all final compounds, more details to SPR screening results, DSF screening results and FP assay condition optimizations as well as concentration dependent FP experiments of compounds **37**, **41**-**43**, **47** and **50**., EMSA row data for compounds **37**, **41**-**43**, **47** and **50**, concentration-dependent EMSA for compound **50** and further STD NMR spectra for compounds **41** and **47**, PDB files for the docking results reported in Figure 7 (PDF), molecular formular strings and some data (CSV)are available.

AUTHOR INFORMATION

Corresponding Author

*Phone +(49) 681 988062031; Email: Martin.Empting@helmholtz-hzi.de

Author Contributions

All authors have given approval to the final version of the manuscript

Funding Sources

This work was financial supported by the German Centre for Infection Research (DZIF) and the DFG Collaborative Research Centre 900, project C1.

Notes

The authors declare no competing financial interest.

ACKNOWLEDGMENT

We thank Prof. Dr. Rolf W. Hartmann for his continuous support and guiding expertise. For the help with the SPR and DSF screening we thank Dr. Elisabeth Weidel and for helping with the establishment of the FP-based assay Dr. Christine Maurer and Dr. Jan Hellert.

ABBREVIATIONS USED

AcOH, acetic acid; Ac_2O, acetic anhydride; AIDS-KS, Acquired Immune Deficiency Syndrome-related Kaposi's sarcoma; CTD, *C*-terminal domain; DCM, dichloromethane; DMSO, dimethylsulfoxide; DNA, deoxyribonucleic acid; DBD, DNA binding domain; DMF, dimethylformamid; DIPEA, Diisopropylethylamin; DSF, differential scanning fluorimetry; EBV, Epstein-Barr virus; EBNA1, Epstein-Barr nuclear antigen 1; EDC, 1-ethyl-3-(3-dimethylaminopropyl) carbodiimide hydrochloride; EE, ethyl acetate; EtOH, ethanol; EMSA, electrophoretic mobility shift assay; FA, formic acid; FP, fluorescence polarization; HPLC, high pressure liquid chromatography; HHV-8, human herpesvirus-8; KS, Kaposi Sarcoma; KSHV,

Kaposi´s Sarcoma-associated Herpesvirus; LANA, latency associated nuclear antigen; LBS, LANA binding site; LE, ligand efficiency; LCMS, liquid chromatography mass spectrometer; MeCN, acetonitrile; MeOH, methanol; MST, microscale thermophoresis; NHS, *N*-hydroxy succinimide; PBS, phosphate buffered saline; PE, petroleum benzene; STD NMR, saturation transfer difference Nuclear Magnetic Resonance; SPR, surface plasmon resonance; TBHP, tert-butyl hydroperoxide; *tert*-BuOH, *tert*-butanol; $TMSN_3$, trimethylsilyl azide; TSA, thermal shift assay; TR, terminal repeat.

REFERENCES

(1) World Health Organization - International Agency for Research on Cancer. *A Review of Human Carcinogens;* Lyon, France, 2012; Vol 100 B.

(2) Weidner-Glunde, M.; Mariggiò, G.; Schulz, T. F. Kaposi's sarcoma-associated herpesvirus latency-associated nuclear antigen: replicating and shielding viral DNA during viral persistence. *J. Virol.* **2017,** *91*, 1–10.

(3) Mariggiò, G.; Koch, S.; Schulz, T. F. Kaposi sarcoma herpesvirus pathogenesis. *Philos. Trans. R. Soc. Lond. ,. B,. Biol. Sci.* **2017,** *372*, 1–20.

(4) Rainbow, L.; Platt, G. M.; Simpson, G. R.; Sarid, R.; Gao, S. J.; Stoiber, H.; Herrington, C. S.; Moore, P. S.; Schulz, T. F. The 222- to 234-kilodalton latent nuclear protein (LNA) of kaposi's sarcoma-associated herpesvirus (human herpesvirus 8) is encoded by orf73 and is a component of the latency-associated nuclear antigen. *J. Virol.* **1997,** *71*, 5915–5921.

(5) Kedes, D. H.; Ganem, D.; Ameli, N.; Bacchetti, P.; Greenblatt, R. The prevalence of serum antibody to human herpesvirus 8 (kaposi sarcoma-associated herpesvirus) among HIV-seropositive and high-risk HIV-seronegative women. *JAMA* **1997,** *277*, 478–481.

(6) Verma, S. C.; Lan, K.; Robertson, E. Structure and function of latency-associated nuclear antigen. *Curr. Top. Microbiol. Immunol.,* **2007,** *312*, 101–136.

(7) Hellert, J.; Weidner-Glunde, M.; Krausze, J.; Lünsdorf, H.; Ritter, C.; Schulz, T. F.; Lührs, T. The 3D structure of kaposi sarcoma herpesvirus LANA C-terminal domain bound to DNA. *Proc. Natl. Acad. Sci. U. S. A.* **2015,** *112*, 6694–6699.

(8) Barbera, A. J.; Chodaparambil, J. V.; Kelley-Clarke, B.; Joukov, V.; Walter, J. C.; Luger, K.; Kaye, K. M. The nucleosomal surface as a docking station for kaposi's sarcoma herpesvirus LANA. *Science* **2006,** *311*, 856–861.

(9) Chodaparambil, J. V.; Barbera, A. J.; Lu, X.; Kaye, K. M.; Hansen, J. C.; Luger, K. A charged and contoured surface on the nucleosome regulates chromatin compaction. *Nat. Struct. Mol. Biol.* **2007,** *14*, 1105–1107.

(10) Alkharsah, K. R.; Schulz, T. F. A role for the internal repeat of the kaposi's sarcoma-associated herpesvirus latent nuclear antigen in the persistence of an episomal viral genome. *J. Virol.* **2012,** *86*, 1883–1887.

(11) Russo, J. J.; Bohenzky, R. A.; Chien, M.-C.; Chen, J.; Yan, M.; Maddalena, D.; Parry, J. P.; Peruzzi, D.; Edelman, I. S.; Chang, Y.; Moore, P. S. Nucleotide sequence of the kaposi sarcoma-associated herpesvirus (HHV8). *Proc. Natl. Acad. Sci. U. S. A.* **1996,** *93*, 14862–14867.

(12) Coen, N.; Duraffour, S.; Snoeck, R.; Andrei, G. KSHV targeted therapy: an update on inhibitors of viral lytic replication. *Viruses* **2014,** *6*, 4731–4759.

(13) Li, N.; Thompson, S.; Schultz, D. C.; Zhu, W.; Jiang, H.; Luo, C.; Lieberman, P. M. Discovery of selective inhibitors against EBNA1 via high throughput in silico virtual screening. *PLoS ONE* **2010,** *5*, e10126.

(14) Hellert, J.; Weidner-Glunde, M.; Krausze, J.; Richter, U.; Adler, H.; Fedorov, R.; Pietrek, M.; Rückert, J.; Ritter, C.; Schulz, T. F.; Lührs, T. A structural basis for BRD2/4-mediated host chromatin interaction and oligomer assembly of kaposi sarcoma-associated herpesvirus and murine gammaherpesvirus LANA proteins. *PLoS Pathog.* **2013,** *9*, e1003640.

(15) Maurer, C. K.; Fruth, M.; Empting, M.; Avrutina, O.; Hoßmann, J.; Nadmid, S.; Gorges, J.; Herrmann, J.; Kazmaier, U.; Dersch, P.; Müller, R.; Hartmann, R. W. Discovery of the first small-molecule CsrA-RNA interaction inhibitors using biophysical screening technologies. *Future Med. Chem.* **2016,** *8*, 931–947.

(16) Weidel, E.; Negri, M.; Empting, M.; Hinsberger, S.; Hartmann, R. W. Composing compound libraries for hit discovery-rationality-driven preselection or random choice by structural diversity? *Future Med. Chem.* **2014,** *6*, 2057–2072.

(17) Cimmperman, P.; Baranauskiene, L.; Jachimoviciūte, S.; Jachno, J.; Torresan, J.; Michailoviene, V.; Matuliene, J.; Sereikaite, J.; Bumelis, V.; Matulis, D. A quantitative model of thermal stabilization and destabilization of proteins by ligands. *Biophys. J.* **2008,** *95*, 3222–3231.

(18) Lea, W. A.; Simeonov, A. Fluorescence polarization assays in small molecule screening. *Expert Opin. Drug Discov.* **2011,** *6*, 17–32.

(19) Hellert, J.; Krausze, J.; Schulz, T. F.; Lührs, T. Crystallization, room-temperature X-ray diffraction and preliminary analysis of kaposi's sarcoma herpesvirus LANA bound to DNA. *Acta Crystallogr. F Struct. Biol. Commun.* **2014,** *70*, 1570–1574.

(20) Wang, X.; Jin, Y.; Zhao, Y.; Zhu, L.; Fu, H. Copper-catalyzed aerobic oxidative intramolecular C-H amination leading to imidazobenzimidazole derivatives. *Org. Lett.* **2012,** *14*, 452–455.

(21) Campiani, G.; Morelli, E.; Gemma, S.; Nacci, V.; Butini, S.; Hamon, M.; Novellino, E.; Greco, G.; Cagnotto, A.; Goegan, M.; Cervo, L.; Dalla Valle, F.; Fracasso, C.; Caccia, S.; Mennini, T. Pyrroloquinoxaline derivatives as high-affinity and Selective 5-HT 3 receptor agonists: synthesis, further structure−activity relationships, and biological studies. *J. Med. Chem.* **1999,** *42*, 4362–4379.

(22) Lan, J.-B.; Chen, L.; Yu, X.-Q.; You, J.-S.; Xie, R.-G. A simple copper salt catalysed the coupling of imidazole with arylboronic acids in protic solvent. *Chem. Commun. (Camb)* **2004**, 188–189.

(23) Pratt, D. A.; Pesavento, R. P.; van der Donk, W. A. Model studies of the histidine-tyrosine cross-link in cytochrome C oxidase reveal the flexible substituent effect of the imidazole moiety. *Org. Lett.* **2005,** *7*, 2735–2738.

(24) He, Z.; Bae, M.; Wu, J.; Jamison, T. F. Synthesis of highly functionalized polycyclic quinoxaline derivatives using visible-light photoredox catalysis. *Angew. Chem. Int. Ed Engl.* **2014,** *53*, 14451–14455.

(25) Tang, C.; Jiao, N. Copper-catalyzed C-H azidation of anilines under mild conditions. *J. Am. Chem. Soc.* **2012,** *134*, 18924–18927.

(26) Hu, M.; Li, J.; Yao, S. Q. In situ "click" assembly of small molecule matrix metalloprotease inhibitors containing zinc-chelating groups. *Org. Lett.* **2008,** *10*, 5529–5531.

(27) Addy, P. S.; Erickson, S. B.; Italia, J. S.; Chatterjee, A. A chemoselective rapid azo-coupling reaction (CRACR) for unclickable bioconjugation. *J. Am. Chem. Soc.* **2017,** *139*, 11670–11673.

(28) Hou, J.; Liu, X.; Shen, J.; Zhao, G.; Wang, P. G. The impact of click chemistry in medicinal chemistry. *Expert Opin. Drug Discov.* **2012,** *7*, 489–501.

(29) Mortenson, P. N.; Murray, C. W. Assessing the lipophilicity of fragments and early hits. *J. Comput. Aided Mol. Des.* **2011,** *25*, 663–667.

(30) Shargel, L.; Wu-Pong, S.; Yu, A. B. C. *Applied Biopharmaceutics & Pharmacokinetics* 5. ed; McGraw-Hill Medical Publ. Division: New York, NY, **2005**.

(31) Erlanson, D. A.; Jahnke, W., Eds. *Fragment-based Drug Discovery;* Wiley-VCH Verlag GmbH & Co. KGaA: Weinheim, 2016.

(32) Hellman, L. M.; Fried, M. G. Electrophoretic mobility shift assay (EMSA) for detecting protein-nucleic acid interactions. *Nat. Protoc.* **2007,** *2*, 1849–1861.

(33) Jerabek-Willemsen, M.; André, T.; Wanner, R.; Roth, H. M.; Duhr, S.; Baaske, P.; Breitsprecher, D. Microscale thermophoresis: interaction analysis and beyond. *J. Mol. Struct.* **2014,** *1077*, 101–113.

(34) Molecular Operating Environment (MOE), 2013.08 *Chemical computing group ULC* **2018**.

(35) Krieger, E.; Koraimann, G.; Vriend, G. Increasing the precision of comparative models with YASARA NOVA--a self-parameterizing force field. *Proteins* **2002,** *47*, 393–402.

Table of contents graphic